Dynamic Properties of the Guest Molecules in the Pyrazine/α-Zirconium Phosphate Intercalation Compound: a Multinuclear Solid-State NMR Study

Marta Bach-Vergés, Simon J. Kitchin, Gary B. Hix, and Kenneth D. M. Harris*

School of Chemistry, University of Birmingham, Edgbaston, Birmingham B15 2TT, United Kingdom

Abil E. Aliev

Department of Chemistry, University College London, 20 Gordon Street, London WC1H 0AJ, United Kingdom

Received December 26, 2001. Revised Manuscript Received March 21, 2002

Dynamic properties of perdeuterated pyrazine (pyrazine-d_4) guest molecules in the layered α-zirconium phosphate host structure have been established from solid-state ^{2}H NMR line-shape analysis and ^{2}H NMR spin−lattice relaxation time measurements. Both techniques indicate that the intercalation compound contains two different types of pyrazine-d_4 guest molecules, which undergo different dynamic processes. The relative proportions of the two types of pyrazine-d_4 guest molecules are approximately 30% (component A) and 70% (component B). The pyrazine-d_4 molecules representing component B undergo two-site 180° jumps about the N···N axis of the molecule, whereas the pyrazine-d_4 molecules representing component A undergo an effectively isotropic motion. The activation energy for the two-site 180° motion of component B is estimated to be 39 kJ mol^{-1} from the ^{2}H NMR spin−lattice relaxation time measurements and 49 kJ mol^{-1} from the ^{2}H NMR line-shape analysis. Structurally, it may be inferred that component B comprises guest molecules for which the N···N axis has a restricted orientation in space, presumably because of direct interactions with the α-zirconium phosphate host structure, whereas component A comprises guest molecules that are held rather weakly in the host structure (or on its external surfaces) such that their reorientation is relatively unrestricted. Thermogravimetric analysis provides direct evidence for the existence of two different types of pyrazine guest molecules in the α-zirconium phosphate host structure, with different strengths of binding and with populations in the approximate ratio 30:70. High-resolution solid-state ^{15}N NMR and ^{13}C NMR spectra provide further support for the existence of two different types of pyrazine guest species within the α-zirconium phosphate host structure and provide direct evidence that the pyrazine guest molecules of component B are N-protonated (from the host structure).

1. Introduction

α-Zirconium phosphate (abbreviated α-ZrP) is a layered material[1−4] with composition $Zr(HPO_4)_2{\cdot}H_2O$. In the layers, Zr^{4+} ions are coordinated in an octahedral arrangement by oxygen atoms of the $HOPO_3^{2-}$ ions, such that each Zr^{4+} ion is coordinated to six different $HOPO_3^{2-}$ ions. Three oxygen atoms of each $HOPO_3^{2-}$ ion are coordinated to Zr^{4+} ions in this way, and the OH group of each $HOPO_3^{2-}$ ion is pendant between the layers. One of the most widely studied properties of α-ZrP is its ability to act as a host material in intercalation reactions in which neutral "guest" molecules are inserted between the layers. These guest molecules replace the water molecules that are present between the layers in the parent material $Zr(HPO_4)_2{\cdot}H_2O$, although some of the water molecules may remain as co-intercalated species. A wide variety of guest molecules (for example, amines, alcohols, diols, and thiols) have been intercalated in this host structure.

Chart 1. Molecular Structure of Pyrazine-d_4

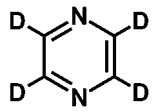

We focus here on the intercalation compound comprising α-ZrP as the host material and pyrazine (Chart 1) as the guest species. In particular, we report solid-state ^{2}H NMR investigations of the dynamic properties of the pyrazine guest molecules within the layered host structure, for the α-ZrP intercalation compound containing perdeuterated pyrazine (pyrazine-d_4) guest mol-

* To whom correspondence should be addressed. Telephone: +44-121-414-7474. Fax: +44-121-414-7473. E-mail: K.D.M.Harris@bham.ac.uk.

(1) Clearfield, A.; Stynes, J. A. *J. Inorg. Nucl. Chem.* **1964**, *26*, 117.
(2) Alberti, G.; Casciola, M.; Costantino, U.; Vivani, R. *Adv. Mater.* **1996**, *8*, 291.
(3) Clearfield, A. *Curr. Opin. Solid State Chem.* **1996**, *1*, 268.
(4) Clearfield, A.; Costantino, U. In *Comprehensive Supramolecular Chemistry*; Alberti, G., Bein, T., Eds.; Pergamon Press: New York, 1996; Vol. 7, p 107.

10.1021/cm0117329 CCC: $22.00
Published on Web 04/24/2002

ecules. ^{2}H NMR spectroscopy is a powerful technique for studying molecular reorientation in solids,[5−10] particularly (in the case of ^{2}H NMR line-shape analysis) when the rate of motion is in the range 10^3-10^7 s^{-1}. Faster rates of motion may be probed using ^{2}H NMR spin−lattice relaxation time (T_1) measurements. In this paper, ^{2}H NMR line-shape analysis is used to investigate the dynamics of the pyrazine-d_4 guest molecules in the α-ZrP host structure, by fitting simulated ^{2}H NMR line shapes for proposed dynamic models to the experimental ^{2}H NMR spectra. Measurements of ^{2}H NMR spin−lattice relaxation times are also used to provide complementary information on the dynamic properties of the pyrazine guest molecules. In addition, high-resolution solid-state ^{13}C and ^{15}N NMR studies provide important supporting evidence concerning structural characteristics of the pyrazine-d_4 guest molecules within this system.

2. Experimental Section

2.1. Synthesis. The pyrazine-d_4/α-ZrP intercalation material was prepared by the following procedure. Pyrazine-d_4 was obtained from Aldrich and used without further purification. Our method for intercalation[11] involved the introduction of the pyrazine-d_4 guest species directly during synthesis of the α-ZrP host structure. In this approach, the "sol−gel" route[12,13] for synthesis of α-ZrP is employed rather than the more commonly used HF route.[14] The sol−gel method involved mixing equal volumes of a phosphoric acid solution (85%) and a solution (1 mol dm^{-3}) of zirconium propoxide in propan-1-ol. A gelatinous precipitate formed immediately and was then kept in contact with the mother liquor at 60 °C for about 1 week. Pyrazine-d_4 was added to the phosphoric acid solution before mixing it with the zirconium propoxide solution. The products were recovered by centrifugation, thoroughly washed with water, and dried in air.

Powder X-ray diffraction indicated that the pyrazine-d_4 guest molecules are intercalated within the layers of the α-ZrP host material, as is evident from an increased interlayer separation in comparison with the parent host material $Zr(HPO_4)_2{\cdot}H_2O$ (typical powder X-ray diffraction patterns for materials prepared by this method are shown in ref 11). The pyrazine/α-ZrP intercalation compound is characterized by the (002) reflection at $2\theta = 8.3°$ in the powder X-ray diffraction pattern (Cu Kα_1 radiation), corresponding to an interlayer distance of 10.65 Å. For comparison, the parent host material $Zr(HPO_4)_2{\cdot}H_2O$ is characterized by the (002) reflection at $2\theta = 11.7°$, corresponding to an interlayer distance of 7.56 Å. Clearly, the intercalation of pyrazine is associated with a significant increase in the interlayer separation in the host material. From the powder X-ray diffraction pattern, we deduce that the pyrazine-d_4/α-ZrP intercalation material prepared in this work had comparatively good crystallinity, with no evidence for any significant amount of an amorphous component. The particle sizes have not been determined in the present work. We recall[15,16] that careful control of the synthetic conditions can have an important bearing on the crystallinity of α-ZrP intercalation materials.

2.2. Solid-State NMR. Solid-state ^{2}H NMR spectra were recorded for a polycrystalline sample of the pyrazine-d_4/α-ZrP intercalation compound in the temperature range 213−383 K using a Chemagnetics CMX-Infinity 300 spectrometer operating at 46.080 MHz. A Chemagnetics single-resonance static 5 mm probe was used. The conventional quadrupole-echo $(90°)_\phi-\tau-(90°)_{\phi\pm\pi/2}-\tau'-$acquire−recycle pulse sequence[17] was used, with a 90° pulse duration of 2 μs, an echo delay τ of 30 μs, and an eight-step phase cycle. At 298 K, further spectra were recorded with different values of the echo delay between 30 and 120 μs. The recycle delay ranged from 4 to 600 s depending on the temperature. For temperatures above 223 K, the recycle delay was longer than $5T_1$, whereas for temperatures below 223 K, the recycle delay was about $3T_1$.

^{2}H NMR spin−lattice relaxation times (T_1) were measured using saturation−recovery and inversion−recovery techniques. Saturation−recovery experiments[18] were carried out in the temperature range 273−403 K using the pulse sequence $[\tau_d-(90°)_x]_n-\tau_r-(90°)_\phi-\tau-(90°)_{\phi\pm\pi/2}-\tau'-$acquire−recycle, where $n = 31$, $\tau_d = 250$ μs, $\tau = 30$ μs, and $\tau_r = t_0[(10)^{1/10}]^{N-1}$, where t_0 is the duration of the first delay and N is the delay number. The data obtained from the saturation−recovery experiments were fitted to multicomponent exponential recovery functions using the spectrometer software. Inversion−recovery experiments were carried out at 298 K using an inversion−recovery pulse sequence modified for ^{2}H nuclei,[19] consisting of a composite inversion pulse followed by quadrupole-echo detection: $[(CP)(\overline{CP})(CP)]_\Phi-\tau_r-(90°)_\phi-\tau-(90°)_{\phi\pm\pi/2}-\tau'-$acquire−recycle, where (CP) ≡ 17°, 62°, 99°, 144° (overbars indicate a 180° phase shift) and $\tau = 30$ μs.

High-resolution solid-state ^{13}C NMR spectra were recorded at 298 K for a polycrystalline sample of the pyrazine-d_4/α-ZrP intercalation compound using a Chemagnetics CMX-Infinity 300 spectrometer operating at 75.489 MHz. A Chemagnetics 4 mm triple-resonance magic-angle-spinning probe was used. Separate spectra were recorded using ^{13}C ← ^{1}H cross-polarization (contact time of 4 ms) and using ^{13}C direct polarization. Because the ^{13}C NMR experiments used pyrazine-d_4/α-ZrP, which contains deuterated guest molecules (i.e., the same material prepared for the ^{2}H NMR studies), the ^{13}C ← ^{1}H cross-polarization will arise from ^{1}H nuclei that originate in the α-ZrP host structure. Both ^{13}C NMR spectra were recorded under conditions of magic-angle sample spinning [spinning frequency of 5000 ± 2 Hz] and high-power ^{1}H decoupling (using the TPPM decoupling sequence;[20] decoupler field strength of ca. 75 kHz). The recycle delay was 6 s for the cross-polarization experiment and 3 s for the direct-polarization experiment. Chemical shifts are reported relative to the ^{13}C resonance in tetramethylsilane. In the case of the ^{13}C direct-polarization experiment, a background suppression sequence[21,22] was employed to suppress the signal from Teflon spacers in the rotor.

A high-resolution solid-state ^{15}N NMR spectrum was recorded at 298 K for a polycrystalline sample of the pyrazine-d_4/α-ZrP intercalation compound using a Bruker MSL300 spectrometer operating at 30.423 MHz. A Bruker 7 mm double-resonance magic-angle-spinning probe was used. The spectrum was recorded under conditions of ^{15}N ← ^{1}H cross-polarization (again, the ^{15}N ← ^{1}H cross-polarization will arise from ^{1}H nuclei that originate in the α-ZrP host structure), magic-angle

(5) Seelig, J. *Quart. Rev. Biophys.* **1977**, *10*, 353.
(6) Jelinski, L. W. *Annu. Rev. Mater. Sci.* **1985**, *15*, 359.
(7) Alam, T. M.; Drobny, G. P. *Chem. Rev.* **1991**, *91*, 1545.
(8) Vold, R. R.; Vold, R. L. *Adv. Magn. Opt. Reson.* **1991**, 85.
(9) Hoatson, G. L.; Vold, R. L. *NMR Basic Principles and Progress*; Springer-Verlag: Berlin, 1994; Vol. 32, pp 3−67.
(10) Vold, R. R. In *Nuclear Magnetic Resonance Probes of Molecular Dynamics*; Tycko, R., Ed.; Kluwer Academic Publishers: Dordrecht, The Netherlands, 1994; pp 27−106.
(11) Hix, G. B.; Harris, K. D. M. *Eur. J. Solid State Inorg. Chem.* **1997**, *34*, 589.
(12) Benhamza, H.; Barboux, P.; Bouhaouss, A.; Josien, F.-A.; Livage, J. *J. Mater. Chem.* **1991**, *1*, 681.
(13) Colomban, P.; Novak, A. *J. Mol. Struct.* **1989**, *198*, 277.
(14) Alberti, G.; Torracca, E. *J. Inorg. Nucl. Chem.* **1968**, *30*, 317.
(15) Clearfield, A.; Berman, J. R. *J. Inorg. Nucl. Chem.* **1981**, *43*, 2141.
(16) Clearfield, A.; Kullberg, L.; Oskarsson, A. *J. Phys. Chem.* **1974**, *78*, 1150.
(17) Davis, J. H.; Jeffrey, K. R.; Bloom, M.; Valic, M. I.; Higgs, T. P. *Chem. Phys. Lett.* **1976**, *42*, 390.
(18) Look, D. C.; Locker, D. R. *Rev. Sci. Instrum.* **1970**, *41*, 250.
(19) Raleigh, D. P.; Olejniczak, E. T.; Griffin, R. G. *J. Magn. Reson.* **1989**, *81*, 445.
(20) Bennett, A. E.; Rienstra, C. M.; Auger, M.; Lakshmi, K. V.; Griffin, R. G. *J. Chem. Phys.* **1995**, *103*, 6951.
(21) Bax, A. *J. Magn. Reson.* **1985**, *65*, 142.
(22) White, J. L.; Beck, L. W.; Ferguson, D. B.; Haw, J. F. *J. Magn. Reson.* **1992**, *100*, 336.

sample spinning [spinning frequency of 5000 ± 2 Hz] and high-power ^{1}H decoupling (decoupler field strength of ca. 50 kHz). The recycle delay was 1 s, and the cross-polarization contact time was 1 ms. Chemical shifts are reported relative to the ^{15}N resonance in CH_3NO_2.

2.3. Simulation of ^{2}H NMR Spectra. Line-shape analysis of the ^{2}H NMR spectra was carried out using the program MXQET.[23] Calculations using MXQET include effects arising from the virtual free induction decay and corrections for imperfect spectral coverage (due to finite pulse power). The latter generally causes a reduction in the intensity of the shoulders of the experimental ^{2}H NMR spectrum. In modeling dynamic processes by jump models, each ^{2}H site involved in the motion is specified by the Euler angles $\{\alpha, \beta, \gamma\}$, which define the orientation (relative to a space-fixed reference frame) of the principal-axis system of the electric field gradient tensor ($\mathbf{V}^{PAS}$) at the ^{2}H nucleus. The components of $\mathbf{V}^{PAS}$ are defined such that $|V_{zz}| \geq |V_{yy}| \geq |V_{xx}|$. The asymmetry parameter η is defined as $(|V_{yy}| - |V_{xx}|)/|V_{zz}|$ (and is in the range $0 \leq \eta \leq 1$), and the quadrupole coupling constant χ is defined as eQV_{zz}/h (where Q is the electric quadrupole moment of the nucleus). The z axis of the $\mathbf{V}^{PAS}$ tensor for each ^{2}H nucleus in the pyrazine-d_4 molecule is assumed to lie along the direction of the C−D bond.

2.4. Thermal Analysis. Thermogravimetric analysis (TGA) of pyrazine-d_4/α-ZrP was carried out on a Perkin-Elmer TGA6 instrument. The sample (7.0 mg) was heated from 273 to 673 K at a rate of 10 K min^{-1}. Differential scanning calorimetry (DSC) data were recorded for pyrazine-d_4/α-ZrP on a Perkin-Elmer Pyris 1 differential scanning calorimeter. The sample (3.9 mg) was cooled from 293 to 100 K at a rate of −10 K min^{-1}.

3. Results and Discussion

3.1. Preliminary Interpretation of ^{2}H NMR Spectra. Quadrupole-echo ^{2}H NMR spectra of pyrazine-d_4/α-ZrP recorded at temperatures between 213 and 383 K are shown in Figure 1. The spectra at the lowest temperatures (213 and 223 K) show the type of line shape expected for pyrazine-d_4 guest molecules in the slow motion regime ($\tau_c \gtrsim 10^{-3}$ s). With an increase in the temperature to 233 K, a narrow line appears at the center of the spectrum, and this narrow line persists at higher temperatures. Thus, at 233 K and higher temperatures, the spectrum clearly consists of two separate components: a broad powder pattern for which the line shape and intensity change substantially with temperature (over the range 223−383 K) and a narrow line which does not change significantly with temperature. Such spectra clearly suggest that there are two "types" of pyrazine-d_4 guest molecules undergoing different dynamic processes. Any exchange between the two types of pyrazine-d_4 guest molecules is presumably slow with respect to the ^{2}H NMR time scale. Subsequently, we refer to the narrow component as component A and the broad component as component B.

As justified fully below, we assign the motion of component A as an essentially isotropic reorientational motion, and we assign the motion of component B as a two-site 180° jump motion about the N···N axis of the pyrazine-d_4 molecule. For component B, we note that if the nitrogen atoms of the pyrazine-d_4 guest molecules are engaged in specific interactions (for example, hydrogen bonding) with the α-ZrP host structure, the orientation of the axis passing through the two nitrogen atoms of the molecule may be fixed relative to the host

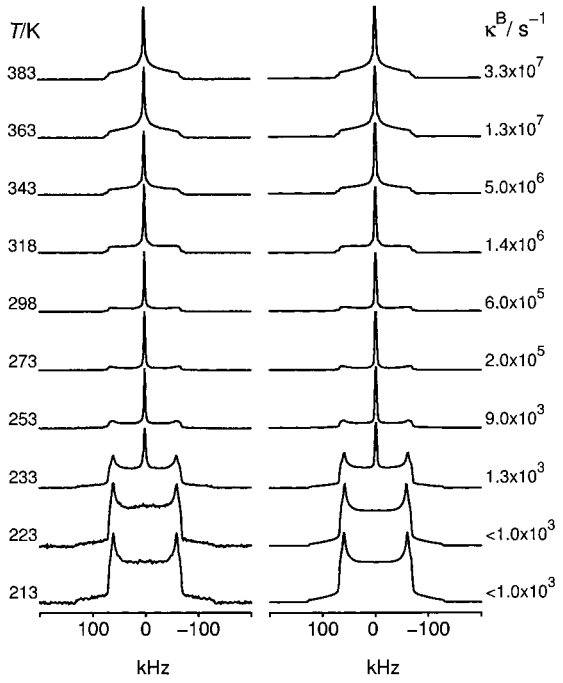

Figure 1. (Left) Experimental ^{2}H NMR spectra recorded for pyrazine-d_4/α-ZrP as a function of temperature using the quadrupole-echo pulse sequence with $\tau = 30$ μs. Note that the spectrum recorded at 213 K has been symmetrized. (Right) The simulated ^{2}H NMR spectrum giving the best fit to the experimental spectrum at each temperature shown. The simulated spectra were calculated using the dynamic models discussed in the text (see Table 2). The jump rate (κ^B) for component B is shown.

structure, and reorientation would be expected to involve rotation about this axis. Given the symmetry of the pyrazine-d_4 molecule, it is reasonable in the first instance to propose that such reorientational motion should take the form of a two-site 180° jump motion about the N···N axis. Clearly, these two different motional models imply that there are two structurally different types of pyrazine-d_4 guest molecules within the α-ZrP host structure and that these different types of guest molecules have significantly different interactions with the host structure. Further experimental evidence concerning the existence and nature of the two different types of guest species is provided in sections 3.4−3.6.

We now consider in detail the ^{2}H NMR spin−lattice relaxation time measurements in section 3.2 and the ^{2}H NMR line-shape analysis in section 3.3.

3.2. ^{2}H NMR Spin−Lattice Relaxation Time Measurements. ^{2}H NMR spectra recorded at 298 K using the inversion−recovery pulse sequence are shown in Figure 2 as a function of the recovery delay τ_r. It is clear that the two parts of the spectrum (the broad powder pattern and the central narrow line) relax independently and are characterized by different spin−lattice relaxation times, confirming that the two parts of the spectrum do indeed represent different dynamic components within the pyrazine-d_4/α-ZrP intercalation compound. The narrow line (component A) exhibits faster recovery from inversion than the broad powder pattern (component B).

To investigate the ^{2}H NMR spin−lattice relaxation behavior as a detailed function of temperature, we have used the saturation−recovery technique. Fitting the

(23) Greenfield, M. S.; Ronemus, A. D.; Vold, R. L.; Vold, R. R.; Ellis, P. D.; Raidy, T. R. *J. Magn. Reson.* **1987**, *72*, 89.

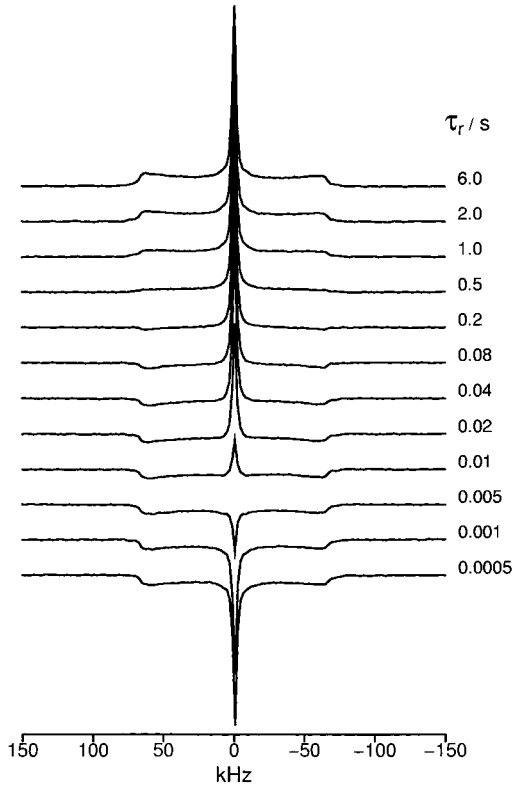

Figure 2. ^{2}H NMR spectra recorded at 298 K using the inversion−recovery technique as a function of the recovery time τ_r. The recovery is faster for the central line (component A) than the broad powder pattern (component B) and is particularly evident from the spectra recorded with τ_r in the range 0.01−0.2 s.

saturation−recovery data to multicomponent exponential recovery functions confirms that there are two separate relaxation processes characterized by different spin−lattice relaxation times [although at the highest temperatures studied (363−383 K), the spin−lattice relaxation times for the two processes have similar values]. From this fitting procedure, we establish that the component with slower relaxation represents about 60% of the pyrazine-d_4 molecules in the sample and the component with faster relaxation represents about 40%. The proportions are essentially independent of temperature. The powder average (denoted $\langle 1/T_1\rangle_p$) of the reciprocal of the ^{2}H NMR spin−lattice relaxation time was measured from the saturation−recovery data. If the temperature dependence of the correlation time τ_c exhibits Arrhenius behavior [i.e., $\tau_c = \tau_0 \exp(E_a/k_B T)$, where E_a denotes the activation energy], it can be shown (for example, using eqs 1−3 discussed later) that in the "extreme narrowing" limit (i.e., $\omega_0\tau_c \ll 1$), a graph of $\ln[(\langle 1/T_1\rangle_p)^{-1}/\mathrm{s}]$ versus T^{-1}/K^{-1} should be a straight line with gradient $-E_a/R$, whereas for the so-called "rigid lattice" limit (i.e., $\omega_0\tau_c \gg 1$), a graph of $\ln[(\langle 1/T_1\rangle_p)^{-1}/\mathrm{s}]$ versus T^{-1}/K^{-1} should be a straight line with gradient $+E_a/R$. The spin−lattice relaxation time data for component B are clearly in the limit corresponding to $\omega_0\tau_c \gg 1$, and from the plot of $\ln[(\langle 1/T_1\rangle_p)^{-1}/\mathrm{s}]$ versus T^{-1}/K^{-1} shown in Figure 3, the activation energy for component B is estimated to be 39 kJ mol^{-1}. For component A, the activation energy is clearly too low to be estimated reliably from these data (see Figure 3).

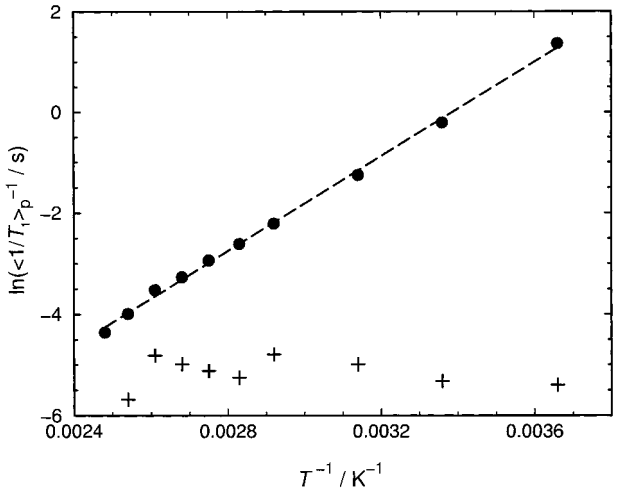

Figure 3. Graphs of $\ln[(\langle 1/T_1\rangle_p)^{-1}/\mathrm{s}]$ versus T^{-1}/K^{-1} for component A (+) and component B (●). The spin−lattice relaxation times were determined from a two-component fit to the saturation−recovery data.

To determine the correlation times (τ_c) for the motions of components A and B at each temperature studied, the equations described below have been used. Note that, because the spin−lattice relaxation behavior has no significant anisotropy (see Figure 2), analysis of the experimental data using expressions for the powder average $\langle 1/T_1\rangle_p$ represents a good approximation. For isotropic motion,[24] $\langle 1/T_1\rangle_p$ is given by the equation

$$\langle 1/T_1\rangle_p = \frac{3\pi^2\chi^2}{10}\left(1+\frac{\eta^2}{3}\right)[J_1(\omega_0) + 4J_2(2\omega_0)] \quad (1)$$

and for a two-site 180° jump motion,[7] $\langle 1/T_1\rangle_p$ is given (under the approximation that $\eta \approx 0$) by the equation

$$\langle 1/T_1\rangle_p = \frac{9\pi^2\chi^2}{10} p_{eq}(1)\, p_{eq}(2)\, \sin^2(2\theta)[J_1(\omega_0) + 4J_2(2\omega_0)] \quad (2)$$

In these expressions,

$$J_m(m\omega_0) = \frac{\tau_c}{1+(m\omega_0\tau_c)^2} \quad (3)$$

and ω_0 denotes the Larmor frequency of the ^{2}H nucleus. The quadrupole coupling constant χ was determined in the present case from the ^{2}H NMR line-shape analysis discussed in section 3.3. For the two-site 180° jump motion, $p_{eq}(1)$ and $p_{eq}(2)$ denote the relative populations of the two sites and θ denotes the angle between the jump axis and the principal axis of the electric field gradient tensor at the ^{2}H nucleus (which is assumed to be parallel to the C−D bond). For the two-site 180° jump motion, the jump frequency κ and correlation time τ_c are related by $\tau_c = (2\kappa)^{-1}$. For the two-site 180° jump motion, we have assumed that the populations of the two sites involved are equal; i.e., $p_{eq}(1) = p_{eq}(2) = {}^1/_2$ in eq 2. Furthermore, the use of eq 2 assumes that the rates of any librational motions around the potential

(24) Spiess, H. W. *NMR Basic Principles and Progress*; Springer-Verlag: Berlin, 1978.

Table 1. Jump Rates (Denoted as κ^B) for Component B Derived from the Values of Correlation Time τ_c Determined from the Spin−Lattice Relaxation Time Data ($\kappa^B = 1/2\tau_c$)[a]

T/K	κ^B/s^{-1}	T/K	κ^B/s^{-1}	T/K	κ^B/s^{-1}
393	2.4×10^7	363	8.4×10^6	318	1.6×10^6
383	1.5×10^7	353	6.1×10^6	295	5.5×10^5
373	1.2×10^7	348	4.3×10^6	273	1.1×10^5

[a] Note that the values of κ^B determined from the fitting procedure at temperatures above ca. 363 K are considered to be less reliable because the values of T_1 for components A and B are close to each other (see Figure 3).

minima are too high and their amplitudes are too low to affect the spin−lattice relaxation.

When eqs 1 and 2 are applied to the experimental data, the correlation times (τ_c) for the motions of components A and B have been determined (and hence also the jump rate κ^B for component B). From these results, it is clear that the motion causing the relaxation for component B is in the intermediate motion regime (10^{-7} s $\lesssim \tau_c \lesssim 10^{-3}$ s) and the motion causing the relaxation for component A is in the rapid motion regime ($\tau_c \lesssim 10^{-7}$ s) throughout the temperature range from 273 to 403 K. The values of κ^B determined in this way from the spin−lattice relaxation data are shown in Table 1 and are consistent, within experimental errors, with the values of κ^B obtained from the ^{2}H NMR line-shape analysis discussed in section 3.3 (although we note that it is only over a restricted set of temperatures that κ^B has been determined by both techniques).

3.3. ^{2}H NMR Line-Shape Analysis. It is clear from the spin−lattice relaxation time measurements and from qualitative inspection of the ^{2}H NMR line shapes (see section 3.1) that the pyrazine-d_4/α-ZrP intercalation compound contains two different types of pyrazine-d_4 guest molecules with distinguishable dynamic properties. In our quantitative analysis of the ^{2}H NMR line shapes, different dynamic models have been used for component A (short T_1) and component B (long T_1).

For component A, the narrow line in the spectrum at 233 K and higher temperatures is characteristic of an effectively isotropic motion and has been simulated using an isotropic line shape in the rapid motion regime ($\kappa^A \gtrsim 10^7$ s^{-1}).

For component B, we consider a two-site 180° jump motion about an axis passing through the two nitrogen atoms of the pyrazine-d_4 molecule, with equal probabilities for the two orientations of the molecule. Assuming that there is no distortion of the pyrazine-d_4 molecules from D_{2h} symmetry, the angle (θ) between the jump axis (N···N axis) and the C−D bond is the same for all ^{2}H nuclei in the molecule. From the molecular geometry, the angle θ should be close to 60°. However, because it is known that the ^{2}H NMR line shape for a two-site 180° jump motion in which θ is close to the magic angle is very sensitive to the actual value of θ, the angle θ was included as a variable in fitting the experimental line shape recorded at 298 K. The best-fit value of θ was 57.5° and is close to the value (57.9°) calculated from the crystal structure of pyrazine (determined at 184 K from a detailed analysis of single-crystal X-ray diffraction data[25]). This value of θ was then kept fixed in fitting the experimental line shapes recorded at all other temperatures. The variable-fitting parameters for component B were, therefore, the rate (κ^B) of the two-site 180° jump motion, the quadrupole coupling constant χ, and the asymmetry parameter η. We note that no significant temperature dependence was found for χ and η.

Table 2. Parameters Used To Calculate the Best-Fit Simulated ^{2}H NMR Line-Shape at Each Temperature[a]

T/K	χ/kHz	η	κ^B/s^{-1}	p_B
383	167	0.06	3.3×10^7	0.69
363	167	0.06	1.3×10^7	0.72
343	167	0.06	5.0×10^6	0.70
318	168	0.06	1.4×10^6	0.75
298	168	0.06	6.0×10^5	0.69
273	170	0.06	2.0×10^5	0.70
253	169	0.06	9.0×10^3	0.70
233	168	0.07	1.3×10^3	0.69
223	168	0.07	SMR	
213	168	0.07	SMR	

[a] κ^B denotes the rate of the two-site 180° jump motion for component B, p_B denotes the proportion of pyrazine-d_4 molecules representing component B, χ is the quadrupole coupling constant, η is the asymmetry parameter, and SMR denotes the slow motion regime ($\kappa^B \lesssim 10^3$ s^{-1}).

The experimental ^{2}H NMR line shapes were fitted by summing ^{2}H NMR spectra simulated using the dynamic models described above for components A and B. To fit the overall experimental line shape, the ratio of the numbers of deuterons representing components A and B was treated as a variable in the fitting process, together with the rate (κ^B) of the two-site 180° jump motion of component B, and the quadrupole interaction parameters χ and η. Because the motion of component A is in the rapid regime, no variables describing this motion were required to be introduced in the simulations. We note that the simulation of the contribution to the line shape from component B implicitly takes into account the attenuation of intensity within the intermediate motion regime.

By finding the simulated line shape that gives the best fit to the experimental line shape recorded at each temperature, the jump rate κ^B for component B has been determined as a function of temperature (see Table 2 and Figure 1). Thus, κ^B increases from the slow motion regime ($\kappa^B \lesssim 10^3$ s^{-1}) at 213 K to 3.3×10^7 s^{-1} at 383 K, covering virtually the full range of the intermediate motion regime. Below 213 K, the motion enters the slow motion regime and a "static" ^{2}H NMR line shape is observed. The graph of $\ln(\kappa^B/\text{s}^{-1})$ versus T^{-1}/K^{-1} (shown in Figure 4) is linear, and assuming Arrhenius behavior for the temperature dependence of κ^B, the activation energy is estimated to be 49 kJ mol^{-1}. This value is comparatively close to that obtained from the spin−lattice relaxation time measurements for component B (see section 3.2).

From the line-shape fitting, the ratio of the two components was found to be essentially constant over the temperature range studied, with about 70% of component B and 30% of component A. Within experimental errors, this result is in broad agreement with the ratio obtained from the spin−lattice relaxation time data.

Component A is in the rapid motion regime ($\kappa^A \gtrsim 10^7$ s^{-1}) at temperatures down to 233 K. At 223 and 213 K, only the powder pattern of component B is readily

(25) De With, G.; Harkema, S.; Feil, D. *Acta Crystallogr.* **1976**, *B32*, 3178.

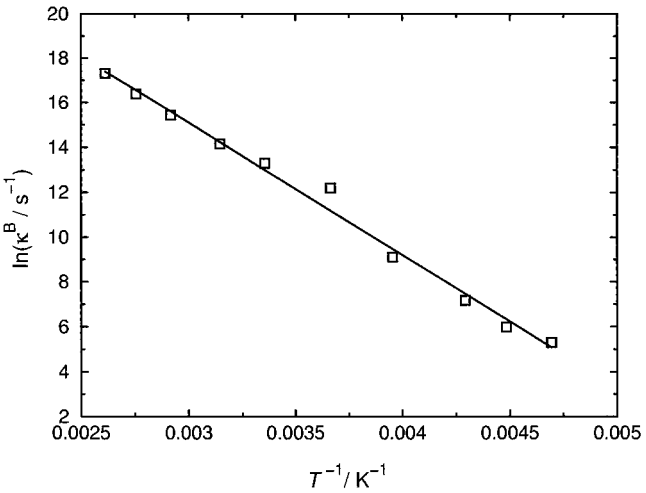

Figure 4. Graph of $\ln(\kappa^B/s^{-1})$ versus T^{-1}/K^{-1} for the two-site 180° jump motion of component B, using values of $\kappa^B(T)$ obtained from the ^2H NMR line-shape analysis.

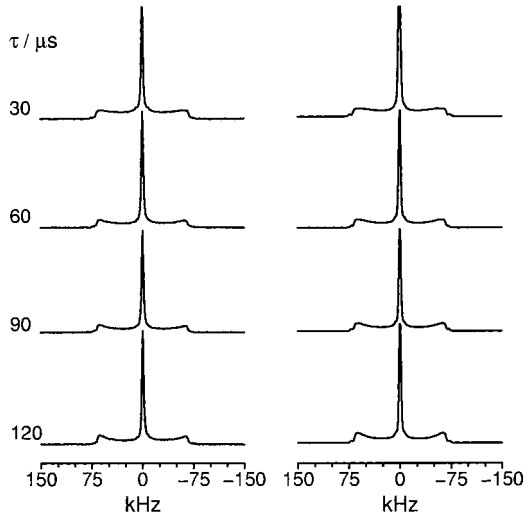

Figure 5. Experimental ^2H NMR spectra (left) recorded at 298 K for different values of the τ delay in the quadrupole-echo pulse sequence and the corresponding simulated ^2H NMR spectra (right). The simulated spectra were calculated using the parameters shown for 298 K in Table 2, except for the different value of the τ delay. Note that the major change in the spectrum as τ is varied concerns the shape in the region of the "maxima" in the line shape of the broad component.

distinguished in the experimental ^2H NMR spectrum. At these temperatures, the powder pattern of component A has broadened to an extent that it has become indiscernible in superposition with the powder pattern from component B (which represents a greater number of deuterons). Thus, from the lack of evidence available, we do not speculate on the dynamic character of component A in this low-temperature range.

In summary, the combination of the dynamic models for components A and B gives good agreement between simulated and experimental ^2H NMR line shapes over the complete temperature range studied (Figure 1). Furthermore, several spectra were recorded at 298 K for different values of the echo delay τ in the quadrupole-echo pulse sequence between 30 and 120 μs. As shown in Figure 5, there is good agreement between the simulated and experimental ^2H NMR line shapes as a function of τ (note that the simulated spectra in Figure 5 were calculated with all parameters fixed at the values established for $\tau = 30$ μs, and only the value of τ was changed). This result further supports our assignment of the dynamic processes in this system.

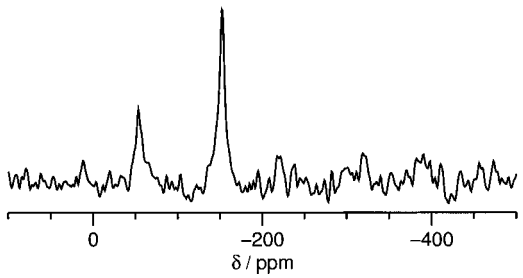

Figure 6. High-resolution solid-state ^{15}N NMR spectrum recorded for pyrazine-d_4/α-ZrP at 298 K using $^{15}N \leftarrow {}^1H$ cross-polarization.

3.4. ^{15}N NMR. The high-resolution solid-state ^{15}N NMR spectrum recorded for pyrazine-d_4/α-ZrP is shown in Figure 6. Although the spectrum was recorded with $^{15}N \leftarrow {}^1H$ cross-polarization over a period of 2.6 days, the signal-to-noise level is still relatively poor (we recall that the natural abundance of the ^{15}N isotope is 0.37% and the receptivity relative to ^1H NMR is only 3.85×10^{-6}). Nevertheless, two isotropic peaks are clearly discernible above the noise level at −53.0 and −152.5 ppm. These peaks may be assigned as non-protonated and protonated ^{15}N nuclei in pyrazine-d_4, respectively. For comparison, the isotropic ^{15}N chemical shifts in pyridine (liquid) and N-protonated pyridine are reported[26] to be −63.2 and −165.2 ppm, respectively. The ^{15}N NMR spectra recorded under conditions of $^{15}N \leftarrow {}^1H$ cross-polarization are not necessarily quantitative, and we may propose (partly in conjunction with the ^{13}C NMR results discussed in section 3.5) that the two signals observed are due to the pyrazine-d_4 molecules representing component B (i.e., the component present in higher amount) in the pyrazine/α-ZrP intercalation compound and that these molecules are protonated on one nitrogen atom as a consequence of proton transfer from the α-ZrP host structure. We note that N-protonation of the pyrazine-d_4 guest molecules will be with ^1H rather than ^2H nuclei, as the ^2H nuclei on the pyrazine-d_4 guest molecules are not expected to undergo any substantial exchange with the ^1H (natural abundance) nuclei of the α-ZrP host structure. It is well-known that pyrazine is essentially a monobasic compound; thus, while N-protonation can occur readily, N,N′-diprotonation occurs only under conditions of very strong acidity. Thus, within the α-ZrP host structure, no significant amounts of N,N′-diprotonated pyrazine are expected to be present.

As concluded from our discussion of the dynamic properties (sections 3.2 and 3.3), it is reasonable to propose that the pyrazine-d_4 guest molecules representing component B engage in hydrogen-bonding interactions with the α-ZrP host structure such that the orientation of the N···N axis of these pyrazine-d_4 guest molecule is essentially fixed in space. Clearly, N−H···O hydrogen-bonding interactions involving a protonated pyrazine-d_4 guest molecule and oxygen atoms of the

(26) Levy, G. C.; Lichter, R. L. *Nitrogen-15 Nuclear Magnetic Resonance Spectroscopy*; John Wiley & Sons: New York, 1979.

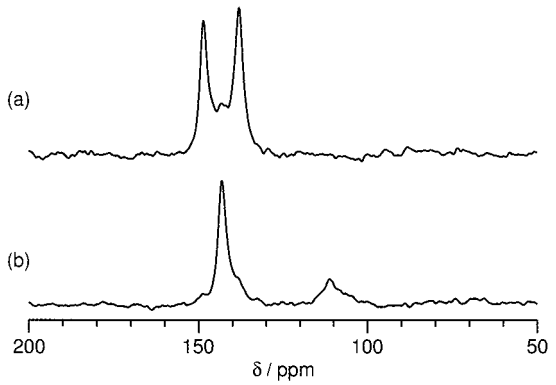

Figure 7. High-resolution solid-state ^{13}C NMR spectra recorded for pyrazine-d_4/α-ZrP at 298 K: (a) with $^{13}C \leftarrow {}^{1}H$ cross-polarization and (b) with ^{13}C direct polarization. The broad peak observed at ca. 110 ppm in the ^{13}C direct polarization spectrum is due to the presence of Teflon spacers in the rotor.

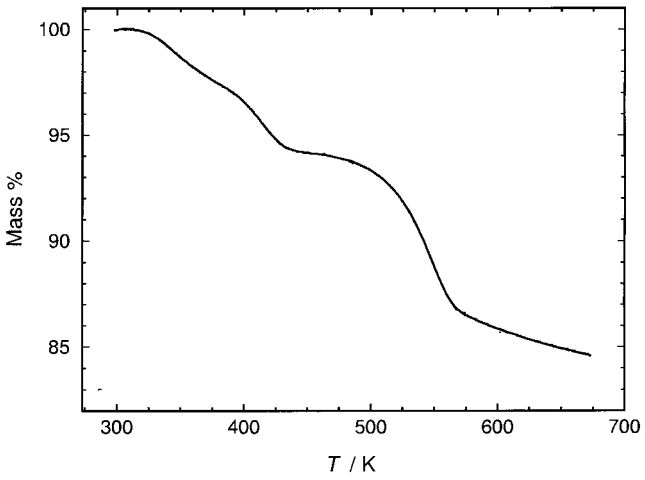

Figure 8. TGA data for pyrazine-d_4/α-ZrP recorded at a heating rate of 10 K min^{-1}.

α-ZrP host structure represent one possible form of such interactions.

The inability to observe a discernible signal in the ^{15}N NMR spectrum due to component A may reflect the lower amount of this component or may reflect substantially different $^{15}N \leftarrow {}^{1}H$ cross-polarization characteristics for the pyrazine-d_4 molecules representing components A and B. In this system, different $^{15}N \leftarrow {}^{1}H$ cross-polarization characteristics for components A and B may originate as a consequence of their different dynamic properties and/or as a consequence of the protonation (by ^{1}H) of the pyrazine-d_4 molecules representing component B, which provides the opportunity for intramolecular $^{15}N \leftarrow {}^{1}H$ cross-polarization (in contrast, molecules of component A, which we propose are nonprotonated, must rely upon intermolecular $^{15}N \leftarrow {}^{1}H$ cross-polarization). The fact that the two ^{15}N signals observed in the spectrum have significantly different intensities presumably arises from the expected differences in the $^{15}N \leftarrow {}^{1}H$ cross-polarization characteristics for protonated (i.e., directly bonded $^{15}N-{}^{1}H$) and nonprotonated ^{15}N environments in the pyrazine-d_4 molecules representing component B.

3.5. ^{13}C NMR. The high-resolution solid-state ^{13}C NMR spectrum (Figure 7a) recorded for pyrazine-d_4/α-ZrP under conditions of $^{13}C \leftarrow {}^{1}H$ cross-polarization contains three isotropic peaks at 148.6, 143.2, and 138.0 ppm. The peaks at 148.6 and 138.0 ppm have essentially the same intensity, which is greater than the intensity of the peak at 143.2 ppm (at the specific cross-polarization contact time used). In contrast, the high-resolution solid-state ^{13}C NMR spectrum (Figure 7b) recorded under conditions of ^{13}C direct polarization (with a recycle delay of 3 s) contains only one isotropic peak at 143.2 ppm. These observations are readily reconciled with the existence of the two different types of guest species introduced in the discussion of the ^{2}H NMR results, and the proposal from our ^{15}N NMR studies that the pyrazine-d_4 guest molecules representing component B are protonated on one nitrogen atom, thus giving rise to two different ^{13}C environments in these molecules. Thus, the three isotropic peaks may be assigned to the two ^{13}C environments in component B and the single (time-averaged) ^{13}C environment in component A. The fact that only one isotropic peak (at 143.2 ppm) is observed in the ^{13}C direct polarization experiment may be attributed to differences in the ^{13}C spin−lattice relaxation times for components A and B, such that, with the comparatively short recycle delay used to record this spectrum, only the component with shorter ^{13}C spin−lattice relaxation time (in general, the component undergoing the faster dynamic process, i.e., component A) is observed in the spectrum. On this basis, the isotropic peak at 143.2 ppm is attributed to component A, and the isotropic peaks at 148.6 and 138.0 ppm are attributed to component B. It is clear that proton exchange between the N-protonated pyrazine-d_4 guest molecules and the α-ZrP host structure and/or between different pyrazine-d_4 guest molecules must be slow with respect to the ^{13}C NMR time scale.

3.6. Thermal Analysis. The results of TGA are shown in Figure 8 and clearly indicate three separate mass losses. The first step occurs from ca. 320 to 367 K, with a mass loss of 2.6%. The second step occurs from ca. 367 to 443 K with a mass loss of 3.6%. The third step occurs from ca. 443 to 515 K with a mass loss of 8.1%. The first mass loss can be attributed to the removal of water molecules from the structure. As discussed above, water molecules are present in the parent material $Zr(HPO_4)_2 \cdot H_2O$ and are replaced by pyrazine-d_4 molecules during the intercalation process. However, not all of the water molecules are replaced during intercalation, and some water molecules remain as co-intercalated species. The second and third mass losses are attributed to the removal of the pyrazine-d_4 guest molecules, confirming that there are two different types of pyrazine-d_4 molecules in the structure. Overall, the TGA results are consistent with a stoichiometry comprising one pyrazine-d_4 molecule and one water molecule for every two zirconium phosphate units in the pyrazine-d_4/α-ZrP starting material.

The difference in the temperature at which the two types of pyrazine-d_4 guest molecules are lost from the host structure suggests that one type of pyrazine-d_4 guest molecule is held more strongly within the host structure. The less strongly bound pyrazine-d_4 guest molecules are lost at lower temperature in the TGA experiment and may be assigned as component A (for which there is rapid isotropic motion). The more strongly bound pyrazine-d_4 guest molecules are lost at higher

temperature in the TGA experiment and can be assigned as component B. As discussed above, these pyrazine-d_4 molecules undergo 180° flips, which may reflect the formation of specific interactions (e.g., hydrogen bonds) with the host structure. The mass loss at lower temperature represents 31% of the total amount of pyrazine-d_4 guest molecules, and the mass loss at higher temperature represents the remaining 69% of the pyrazine-d_4 guest molecules, in very close agreement with the ratio of components A and B found from the ^{2}H NMR line-shape analysis (and in reasonable agreement with the ratio determined from the spin−lattice relaxation time data).

DSC shows no evidence for any thermal anomalies in the temperature range (100−293 K) studied.

4. Concluding Remarks

Our ^{2}H NMR studies provide clear evidence that there are two different types of pyrazine-d_4 guest molecules in the pyrazine-d_4/α-ZrP intercalation compound, characterized by different dynamic behavior. The relative amounts of the two types of guest molecules are about 30% and 70%. The higher population (component B) comprises guest molecules for which the axis passing through the two nitrogen atoms of the pyrazine-d_4 molecule has a restricted orientation in space, presumably as a consequence of a direct interaction with the α-ZrP host structure. These guest molecules undergo two-site 180° jumps about this molecular axis, with the jump rate ranging from less than 10^3 s^{-1} at 213 K to 3.3×10^7 s^{-1} at 383 K. The lower population (component A) comprises guest molecules that undergo an effectively isotropic motion. These guest molecules are presumably held rather weakly within the host structure or on its external surfaces, such that their reorientation is relatively unrestricted. The two-site 180° jump motion of component B passes through the intermediate motion regime (for ^{2}H NMR line-shape analysis) within the temperature range from 233 to 383 K and enters the slow motion regime below about 233 K. The effectively isotropic motion of component A is in the rapid motion regime at temperatures down to 233 K. The activation energy for the two-site 180° motion of component B is estimated to be 39 kJ mol^{-1} from the ^{2}H NMR spin−lattice relaxation time measurements and 49 kJ mol^{-1} from the ^{2}H NMR line-shape analysis. Results from TGA provide direct evidence for the existence of two different types of pyrazine-d_4 guest molecules in the pyrazine-d_4/α-ZrP intercalation compound, with different strengths of binding and with approximate relative populations of 30% (less strongly bound component) and 70% (more strongly bound component). High-resolution solid-state ^{15}N and ^{13}C NMR spectra provide further support for the existence of two different types of pyrazine-d_4 guest species and provide direct evidence that the pyrazine-d_4 guest molecules of component B are N-protonated (from the α-ZrP host structure). The results from TGA, ^{15}N NMR, and ^{13}C NMR are clearly in good accord with conclusions on the dynamic and structural properties of the pyrazine-d_4/α-ZrP intercalation compound reached from our ^{2}H NMR studies.

Acknowledgment. We are grateful to EPSRC, HEFCE, and Ciba Specialty Chemicals for financial support.

CM0117329